Gas Adsorption, Magnetism and Single-Crystal to Single-Crystal Transformation Studies of a Three-Dimensional Mn(II) Porous Coordination Polymer

ARTICLE *in* CRYSTAL GROWTH & DESIGN · OCTOBER 2014

Impact Factor: 4.89 · DOI: 10.1021/cg500833s

5 AUTHORS, INCLUDING:

Rashmi Avinash Agarwal
Indian Institute of Technology Kanpur
10 PUBLICATIONS **41** CITATIONS
SEE PROFILE

Soumya Mukherjee
Indian Institute of Science Education and Res…
29 PUBLICATIONS **240** CITATIONS
SEE PROFILE

E. Carolina Sañudo
University of Barcelona
103 PUBLICATIONS **2,409** CITATIONS
SEE PROFILE

Parimal K Bharadwaj
Indian Institute of Technology Kanpur
118 PUBLICATIONS **3,695** CITATIONS
SEE PROFILE

CRYSTAL GROWTH & DESIGN

Article

pubs.acs.org/crystal

Gas Adsorption, Magnetism, and Single-Crystal to Single-Crystal Transformation Studies of a Three-Dimensional Mn(II) Porous Coordination Polymer

Rashmi A. Agarwal,[†] Soumya Mukherjee,[‡] E. Carolina Sañudo,[§] Sujit K. Ghosh,[‡] and Parimal K. Bharadwaj*[,†]

[†]Department of Chemistry, Indian Institute of Technology Kanpur, 208016, Kanpur, India

[‡]Department of Chemistry, Indian Institute of Science Education and Research (IISER), Dr. Homi Bhabha Road, Pashan, Pune, Maharashtra 411021, India

[§]Departament de Quımica Inorganica, Universitat de Barcelona, Diagonal, 645, 08028-Barcelona, Spain

Supporting Information

ABSTRACT: A porous coordination polymer $\{[Mn_2(DBIBA)_3]NO_3{\cdot}3DMF{\cdot}4H_2O\}_n$ (**1**) [DBIBAH = 3,5-di(1*H*-benzo[d]imidazol-1-yl)benzoic acid] has been synthesized solvothermally and structurally characterized by single-crystal X-ray diffraction. The following four new coordination polymers $\{[Mn_2(DBIBA)_3]{\cdot}ClO_4{\cdot}DMF{\cdot}H_2O\}_n$ (**2**), $\{[Mn_2(DBIBA)_3]{\cdot}Cl{\cdot}DMF{\cdot}8H_2O\}_n$ (**3**), $\{[Mn_2(DBIBA)_3]{\cdot}NO_3{\cdot}CH_3OH{\cdot}5H_2O\}_n$ (**4**) and $\{[Mn_2(DBIBA)_3]{\cdot}NO_3{\cdot}3CH_3COCH_3{\cdot}7H_2O\}_n$ (**5**) have been synthesized from **1** via anion/solvent exchange protocols in a single-crystal to single-crystal fashion at room temperature. Gas sorption studies for desolvated compounds **1**, **2**, and **3** show that CO_2 uptake capacity is entirely dependent upon the size of the anion present in the framework. Complex **1** also exhibits antiferromagnetic properties below 17 K, confirmed through magnetic susceptibility measurements.

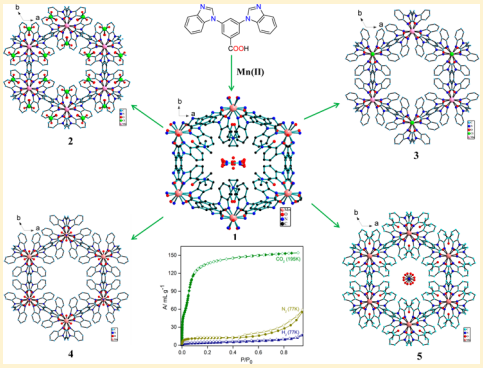

INTRODUCTION

Studies on the functional aspects of porous metal−organic framework materials such as ion exchange,[1,2] separation,[3,4] gas storage,[5−8] sensor and magnetism[9−11] are rapidly emerging. A large number of highly porous metal−organic frameworks (MOFs) have been synthesized which are capable of storing huge amounts of CO_2, as well as significant amounts of other gases.[12] Separation of CO_2 from other gases have high technological and industrial importance.[13,14] The ability to synthesize MOFs with various organic linkers and metal nodes provides tremendous flexibility in tailoring the porous materials to acquire specific physical characteristics and chemical functionalities. For an effective optimized adsorption of CO_2, a periodic porous structure is desirable where uptake and release are fully reversible and flexible, by which chemical functionalization and molecular level fine-tuning can be attained.[15] Meanwhile, carboxylate bridged Mn(II) species are of particular interest, since such systems are known to exist at the active centers of some Mn(II) containing enzymes.[16−19] Besides, high spin Mn(II) contain up to five unpaired electrons; thus the assembly with multicarboxylate is seemingly inclined to the formation of large clusters and extended solids.[20−27] Bulk magnetic properties mainly depend on the bridging modes and the bridging geometry. In recent years, various cyanide, azides, nitrogen-containing aromatic ligands, or carboxylates have been primarily used for the design of hybrid metal−organic compounds with interesting magnetic properties.[28] A great deal of work is essential to understand the underlying structural features that govern the exchange coupling between paramagnetic centers, since such a relationship is complex and has so far remained elusive.[29,30] Self-assembly and its fascinating progress have been highly influenced by several factors, such as the varying counterions, temperature, and solvent, in addition to the nature of metal/ligand.[31−34] Anion exchange has attracted increasing attention in recent years because it opens up novel avenues to constitute such frameworks potentially attractive as anion exchange materials.[35−42] When the framework-open space is occupied by molecular guests, the existing interactions between the host-framework and these guest species are expected to provide useful relationships between the concerned structure and gas sorption properties.[43] Single-crystal to single-crystal (SC−SC) transformation is extremely desirable owing to the systematic study of gas storage and separation, since it allows exact monitoring of how the crystal structure, location, and orientation of guest molecules in the voids is changing during the transformation process in the crystalline phase.[44,45] This can be potentially important in using the coordination space for applications. Herein, we report the

Received: June 7, 2014
Revised: October 13, 2014

   dx.doi.org/10.1021/cg500833s | *Cryst. Growth Des.* XXXX, XXX, XXX−XXX

synthesis and structural characterization of a three-dimensional coordination polymer $\{[Mn_2(DBIBA)_3]NO_3{\cdot}3DMF{\cdot}4H_2O\}_n$ (**1**), synthesized by utilizing a bifurcated ligand consisting of benzimidazole moieties as N donor centers and carboxyl group as O donor centers (Scheme 1). The linker is particularly

Scheme 1. Representation of the Ligand 3,5-Di(1*H*-benzo[d]imidazol-1-yl)benzoic Acid (DBIBAH)

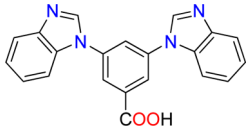

chosen because there is the possibility of rotation about the C−N bond that can allow cooperative movement of the metal-linker ensemble, necessary for SC−SC transformations. Complex **1** affords four new coordination polymers (**2**−**5**) via anion/solvent induced SC−SC transformations. Gas sorption measurements have been performed for desolvated coordination polymers **1**−**3**, and magnetic studies revealed that **1** exhibits antiferromagnetic properties below 17 K.

EXPERIMENTAL SECTION

Materials. Reagent grade 3,5-difluorobenzonitrile and metal salts were acquired from Aldrich and used as received. All solvents, benzimidazole and K_2CO_3 were procured from S. D. Fine Chemicals, India. Solvents were purified prior to use following standard protocols.

Physical Measurements. Infrared spectra were recorded (KBr disk, 400−4000 cm^{-1}) using a PerkinElmer equipment model spectrum version II. ^1H NMR spectra were recorded on a JEOL-ECX 500 FT (500 MHz) in DMSO-d_6 with Me_4Si as the internal standard. ESI mass spectra were recorded on a WATERS Q-TOF premier mass spectrometer. Thermogravimetric analysis data plots were recorded using a Mettler Toledo (heating rate of 5 °C/min) TGA instrument. Powder X-ray diffraction (Cu Kα radiation, scan rate 3°/min, 293 K) was performed on a Bruker D8 Advance Series 2 powder X-ray diffractometer. Low pressure gas sorption measurements were performed using BelSorpmax (Bel Japan). All the gases used were of 99.999% purity. As-synthesized compound **1** was heated at 160 °C under a vacuum for 10 h, to get guest-free compound. Prior to adsorption measurement, the guest-free sample was pretreated at 160 °C under a vacuum for 4 h, using BelPrepvacII, and purged with He on cooling. Similarly, desolvated phases from compounds **2** and **3** were also obtained on heating the as-synthesized phases at 160 °C under a vacuum for 10 h each. Between the experiments with various gases, the outgassing procedure was repeated for ca. 5 h. For low temperature measurements, N_2 and H_2 adsorption isotherms were monitored at 77 K, while CO_2 gas sorption isotherm was monitored at 195 K. The adsorption isotherms at 298 K were monitored individually for the gases, namely, CO_2, N_2, H_2, and CH_4. CO_2 gas sorption isotherm was also measured at 273 K. Surface area and pore size distribution were calculated using BelMaster analysis software package. Magnetic measurements were carried out in the Unitat de Mesures Magnetiques (Universitat de Barcelona) on polycrystalline samples (ca. 30 mg) with a Quantum Design SQUID MPMS-XL magnetometer equipped with a 5 T magnet. Diamagnetic corrections were calculated using Pascal's constant,[46] and an experimental correction factor for the sample holder was applied.

Synthesis of 3,5-Di(1*H*-benzo[d]imidazol-1-yl)benzoic Acid (DBIBAH). In the first step, 5-di(1*H*-benzo[d]imidazol-1-yl)-benzonitrile (DBIBN) was synthesized as previously reported.[47] In the second step, a mixture of DBIBN (2 g, 5.9 mmol) was hydrolyzed by refluxing it with an ethanolic solution of NaOH (0.35 g, 8.8 mmol) for 10 h. Finally, the resulting solution was carefully neutralized with dilute HCl to obtain a pale yellow precipitate. It was collected by filtration, washed thoroughly with water, and air-dried (Scheme 1). Yield: 1.8 g (90%). Melting point: 250 °C; IR (cm^{-1}, KBr pellet): 3403(m), 3086(m), 2421(w), 1895(w), 1704(w), 1645(w), 1605(s), 1501(s), 1473(s), 1396(w), 1244(s), 1213(s), 1167(s), 1135(m), 1091(w), 896(w), 853(w), 782(m), 761(m), 731(s), 690(m), 622(w), 542(w), 489(w), 466(w), 427(w) (Figure S1, Supporting Information). ^1H NMR (DMSO-d_6, 500 MHz) δ (ppm): 8.74 (s, 2H; H_{Ar}), 8.23 (d, 3H; H_{Ar}), 7.77 (m, 4H; H_{Ar}), 7.34 (m, 4H, H_{Ar}) (Figure S2, Supporting Information); ^{13}C NMR (DMSO-d_6) δ (ppm): 166.30, 144.21, 144.06, 138.17, 134.91, 133.26, 124.48, 123.49, 123.36, 123.08, 120.57, 111.35 (Figure S3, Supporting Information). ESI-MS: m/z [M-1] 353.10 (100%); calculated 354.13 (Figure S4, Supporting Information); Anal. Calcd for $C_{21}H_{14}N_4O_2$ (354.13): C, 71.16; H, 3.98; N, 15.82%. Found: C, 70.91; H, 4.07; N, 15.52%.

Synthesis of $\{[Mn_2(DBIBA)_3]{\cdot}NO_3{\cdot}3DMF{\cdot}4H_2O\}_n$ (1). A mixture containing $Mn(NO_3)_2{\cdot}4H_2O$ (0.058 g, 0.22 mmol), DBIBAH (0.04 g, 0.11 mmol) in DMF/H_2O (4 mL, 3:1 v/v) was placed in a Teflon-lined stainless steel autoclave and heated to 80 °C for 2 days under autogenous pressure. Then it was allowed to cool to room temperature at the rate of 1 °C/min. Small light brown crystals of **1** were collected in ∼52% yield. The crystals were repeatedly washed with ethanol and air-dried. Anal. Calcd for $C_{72}H_{68}N_{16}O_{16}Mn_2$: C, 56.75; H, 4.50; N, 14.72%. Found: C, 56.22; H, 4.65; N, 14.82%. IR (cm^{-1}, KBr pellet): 3436(m), 3091(m), 3065(m), 2848(w), 2926(w), 1664(s), 1644(s), 1596(s), 1584(s), 1500(s), 1474(s), 1448(m), 1407(s), 1377(s), 1321(m), 1306(s), 1291(s), 1241(s), 1224(s), 1170(m), 1151(m), 1142(m), 1094(m), 1062(w), 1009(w), 906(m), 872(m), 793(m), 780(s), 766(s), 755(s), 721(s), 689(m), 657(w), 626(w), 610(w), 562(w), 520(w) (Figure S5, Supporting Information).

Synthesis of $\{[Mn_2(DBIBA)_3]{\cdot}ClO_4{\cdot}DMF{\cdot}H_2O\}_n$ (2). Crystals of **1** were immersed in 3 M aqueous solutions of $NaClO_4$ for 1 week at room temperature, upon which **2** was obtained without losing crystallinity. Anal. Calcd for $C_{66}H_{48}N_{13}O_{12}ClMn_2$: C, 58.21; H, 3.56; N, 13.39%. Found: C, 58.3; H, 3.5; N, 13.4%. IR (cm^{-1}, KBr pellet): 3539(m), 3093(m), 1696(m), 1663(m), 1645(s), 1596(s), 1585(s), 1502(s), 1409(s), 1378(s), 1307(s), 1291(s), 1242(s), 1225(s), 1092(s), 765(s), 755(s) (Figure S6).

Synthesis of $\{[Mn_2(DBIBA)_3]{\cdot}Cl{\cdot}DMF{\cdot}8H_2O\}_n$ (3). Crystals of **1** were immersed in 3 M aqueous solutions of NaCl for 1 week at room temperature to obtain **3** without losing crystallinity. Anal. Calcd for $C_{66}H_{62}N_{13}O_{15}ClMn_2$: C, 55.72; H, 4.39; N, 12.80%. Found: C, 55.8; H, 4.4; N, 12.85%. IR (cm^{-1}, KBr pellet): 3417(m), 3067(m), 1663(s), 1643(s), 1595(s), 1499(s), 1404(s), 1375(s), 1241(s), 743(s) (Figure S7).

Synthesis of $\{[Mn_2(DBIBA)_3]{\cdot}NO_3{\cdot}CH_3OH{\cdot}5H_2O\}_n$ (4). Crystals of **1** were dipped in dry methanol for 4 days to obtain **4** without losing crystalinity. Anal. Calcd for $C_{64}H_{53}N_{13}O_{15}Mn_2$: C, 56.77; H, 3.94; N, 13.45%. Found: C, 56.79; H, 3.96; N, 13.47%. IR (cm^{-1}, KBr pellet): 3370(s), 3117(s), 3067(s), 1644(s), 1598(s), 1585(s), 1501(s), 1403(s), 1367(s), 1220(s), 1171(s), 1050(s), 1011(s), 906(s), 882(s), 794(s), 781(s), 746(s), 719(s), 426(s) (Figure S8).

Synthesis of $\{[Mn_2(DBIBA)_3]{\cdot}NO_3{\cdot}3CH_3COCH_3{\cdot}7H_2O\}_n$ (5). Crystals of **1** were dipped in dry acetone for 4 days to obtain **5** in a SC-SC transformation. Anal. Calcd for $C_{72}H_{71}N_{13}O_{22}Mn_2$: C, 54.72; H, 4.53; N, 11.52%. Found: C, 54.74; H, 4.54; N, 11.53%. IR (cm^{-1}, KBr pellet): 3118(m), 1698(w), 1723(w), 1643(s), 1596(s), 1585(s), 1501(s), 1474(s), 1460(s), 1451(s), 1368(s), 1304(s), 1293(s), 1241(s), 1220(s), 1171(m), 1149(m), 1141(m), 1107(m), 906(m), 873(m), 794(m), 781(s), 764(s), 744(s) (Figure S9).

Single Crystal X-ray Studies. Single crystal X-ray data for complexes **1**−**5** were collected at 100 K on a Bruker SMART APEX CCD diffractometer using graphite-monochromated MoK_α radiation (λ = 0.71073 Å) as described earlier.[47] Identification of solvent entities was impossible for **2**−**4** complexes because of disorder contents of the large pores, so squeeze refinements have been performed using PLATON.[48] For compound **5** acetone molecules were located, but water molecules could not be located. Contributions from all atoms of the solvent molecules have been incorporated in both the empirical formulas and formula weights as shown in the crystal and structure refinement data Table. In **1**, all water molecules, nitrate anion and atoms O8, N9, C37, C38, and C39 while in **5** nitrate anion were

dx.doi.org/10.1021/cg500833s | Cryst. Growth Des. XXXX, XXX, XXX−XXX

Table 1. Crystal and Structure Refinement Data for 1−5

	1	2	3	4	5
empirical formula	$C_{72}H_{68}N_{16}O_{16}Mn_2$	$C_{66}H_{48}N_{13}O_{12}ClMn_2$	$C_{66}H_{62}N_{13}O_{15}ClMn_2$	$C_{64}H_{53}N_{13}O_{15}Mn_2$	$C_{72}H_{71}N_{13}O_{22}Mn_2$
formula wt	1523.18	1360.50	1422.61	1354.07	1580.3
crystal system	monoclinic	trigonal	trigonal	trigonal	trigonal
space group	$C2/c$	$P\bar{3}1c$	$P\bar{3}1c$	$P\bar{3}1c$	$P\bar{3}1c$
a, Å	17.966(5)	17.107(5)	17.246(5)	17.485(5)	17.203(5)
b, Å	27.989(5)	17.107(5)	17.246(5)	17.485(5)	17.203(5)
c, Å	14.141(5)	14.133(5)	14.135(5)	14.019(5)	14.045(5)
α (deg)	90.00	90.00	90.00	90.00	90.00
β (deg)	92.381	90.00	90.00	90.00	90.00
γ (deg)	90.00	120.00	120.00	120.00	120.00
U, Å^3	7105(3)	3581.9(19)	3641(2)	3712(2)	3600(2)
Z	4	2	2	2	2
ρ_{calc} g/cm^3	1.410	1.177	1.100	1.102	1.342
μ, mm^{-1}	0.435	0.448	0.434	0.395	0.425
temperature (K)	100	100	100	100	100
θ max	25.50	25.49	25.49	25.49	25.47
F(000)	3100	1296	1232	1260	1500
refl collected	19102	24429	21899	20669	19224
independent refl	4408	1791	1319	1654	1504
GOF	1.036	1.078	1.065	1.098	1.068
final R indices $[I > 2\sigma(I)]$	$R1$ = 0.0789 $wR2$ = 0.1986	$R1$ = 0.0897 $wR2$ = 0.2368	$R1$ = 0.1038 $wR2$ = 0.2486	$R1$ = 0.0597 $wR2$ = 0.1316	$R1$ = 0.0669 $wR2$ = 0.1608
R indices (all data)	$R1$ = 0.1219 $wR2$ = 0.2360	$R1$ = 0.1095 $wR2$ = 0.2519	$R1$ = 0.1791 $wR2$ = 0.2827	$R1$ = 0.0985 $wR2$ = 0.1466	$R1$ = 0.1060 $wR2$ = 0.1815

refined isotropically. Hydrogens could not be located in the difference maps for the three lattice water molecules and a distorted DMF molecule in **1**. Several DFIX and DANG commands were given for nitrate anion of complex **1** and **5** and for perchlorate anion of complex **2**. The absolute value of parameter shift is more than 0.2 for complex **5** which is directly related with the distorted nitrate anion. Because of the poor crystal quality for **2** and **4** the maximum residual density value is remaining high. It was tried with several crystals from different batches but every time was a similar problem. The crystal and refinement data are collected in Table 1, while selective bond angles and bond distances are given in Table S1 in the Supporting Information.

RESULTS AND DISCUSSION

Complex **1** was synthesized under solvothermal conditions at 80 °C by utilizing the DBIBAH ligand. Once isolated, it is found to be stable in air and insoluble in common organic solvents. Single crystal X-ray diffraction analysis reveals that **1** crystallizes in the monoclinic space group $C2/c$, and the asymmetric unit consists of one Mn(II) ion, 1.5 DBIBA ligand, one nitrate anion with half occupancy, one lattice water molecule with full occupancy and two free water molecules with half occupancy, one noncoordinated DMF molecule with full occupancy and another DMF molecule with half occupancy. This DMF molecule is distorted and having translational symmetry passing through its nitrogen atom.

Complex **1** is isostructural to previously reported coordination polymers of Ni(II),[49] Co(II),[47] and Mn(II),[49] but bond angles, torsion and dihedral angles (Figure 1) for **1** vary considerably compared to the reported Mn(II) coordination polymer. Dihedral angle between the two planes of N1 Mn1 O1 and N6 Mn1 O3 is 56.25°, between N1 Mn1 O1 and N4 Mn1 O2 is 81.7°, while that between N4 Mn1 O2 and N6 Mn1 O3 is 86.8°. Torsion angles N1−Mn1−O1−C1, N4−Mn1−O2−C23, and N6−Mn1−O3−C23 are −78.9°, 104.7°, and −51.2° respectively. Along the crystallographic c axis, one-dimensional (1D) channels of diameter ∼5.8 Å (considering van der Waals radii) are present revealing strong $\pi-\pi$ interactions between two benzene rings of two different benzimidazole moieties. Between the two benzene rings of different ligands, DMF molecules are located (Figure 2a). In the center of the cavity, four nitrate anions with six water molecules are present (Figure 2b). These water molecules show significant intermolecular hydrogen bonding interactions with the benzene rings of benzimidazole and hydrogen of methyl group of DMF. Nitrogen atoms of DMF molecule are also involved in hydrogen bonding with central benzene ring hydrogens.

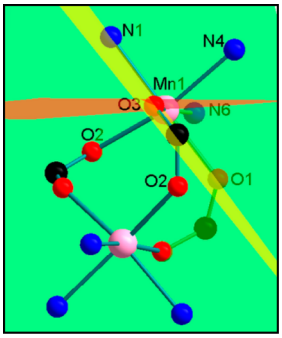

Figure 1. Showing selected planes (N1Mn1 O1, N4Mn1 O2, and N6Mn1 O3) in **1**.

An examination of the packing diagram of **1** along the crystallographic c axis shows the existence of strong hydrogen bonding between nitrate anions, and water molecules (Figure 3). The solvent accessible volume is ∼28.3% of the unit cell volume, calculated from the crystal structure using the PLATON program[48] (Figure S10, Supporting Information).

Single-Crystal to Single-Crystal Transformation Studies. Crystal structure of **1**, consisting nitrate anions, DMF, and water molecules, which are involved in significant hydrogen bonding interactions with the framework, rendering the

dx.doi.org/10.1021/cg500833s | Cryst. Growth Des. XXXX, XXX, XXX−XXX

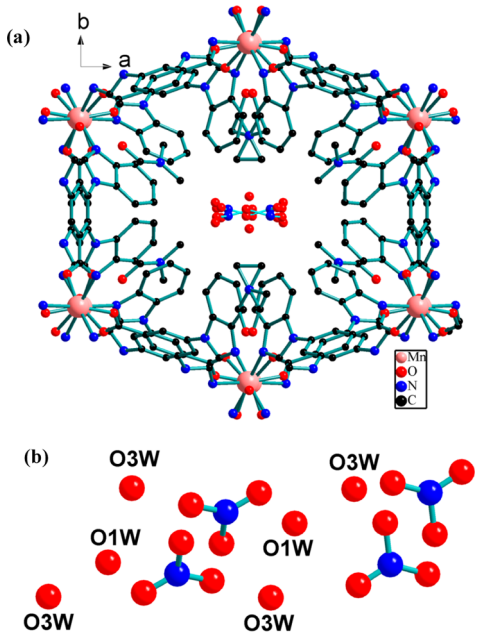

Figure 2. (a) View along the *c* axis showing distorted DMF molecules and nitrate anion (hydrogen atoms are omitted because of clarity) and (b) a perspective view of the central part of cavity.

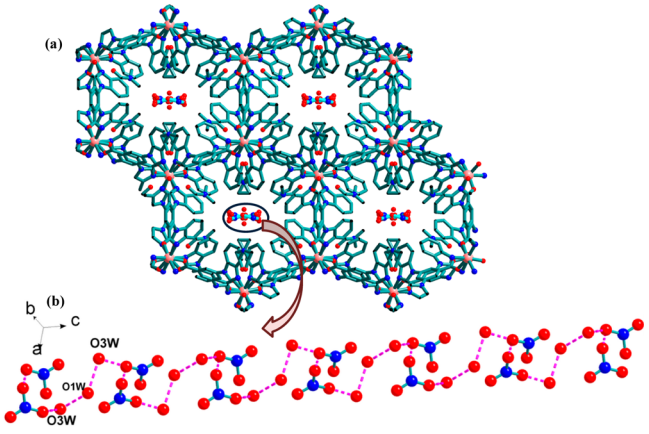

Figure 3. (a) Packing diagram of **1** along the *c* axis (hydrogen atoms are omitted because of clarity) and (b) central unit showing strong hydrogen bonding channel.

framework an ideal candidate for performing anion/solvent exchange studies. A crystal of **1** of suitable size is dipped in 3 M aqueous solution of $NaClO_4$ for 7 days at room temperature. It leads to complete replacement of NO_3^- with the ClO_4^- anion affording compound **2** with retention of crystallinity. A strong peak at 1090 cm^{-1} in the IR spectrum of **2** suggests the presence of free ClO_4^- anion (Figure S6, Supporting Information). Similarly, when a crystal of **1** is dipped in 3 M aqueous solution of NaCl for 7 days at room temperature, complete replacement of NO_3^- by Cl^- occurs to afford compound **3** with retention of crystallinity. This is further supported by the IR spectra where complete disappearance of the NO_3^- peak at 1350 cm^{-1} suggests conversion of **1** into **3** (Figure S7, Supporting Information). Likewise, compounds **4** and **5** can be obtained from **1** in SC−SC fashion by dipping a crystal of **1** in dry methanol and dry acetone, respectively. The IR spectra of **4** and **5** are indicative of the presence of methanol (Figure S8, Supporting Information) and acetone (Figure S9, Supporting Information) respectively. Snapshots were taken before and after each SC−SC transformation reaction (Figure S11, Supporting Information). However, in each case of these SC−SC transformation reactions, the crystal quality is maintained, and there is no change in color and shape.

Crystallographic space group of **1** underwent a clear change from monoclinic $C2/c$ to trigonal $P\bar{3}1c$, in all **1**−**4** complexes. For compound **2**, when viewed along the *c* axis, perchlorate anions in a single cavity remain sandwiched between two benzene rings of different benzimidazole moieties, while in **3**, the chloride ions are present between binuclear cluster units (Figure S12, Supporting Information). Both $\pi-\pi$ and anion$-\pi$ interactions are present in the hexagonal cavity. In **2** and **3**, a view along the crystallographic *a* axis shows perchlorate and chloride ions to be involved in hydrogen bonding interactions with the ligand hydrogens (Figures S13 and S14). In both the structures, metal to anion distance is decreased significantly compared to that of the framework **1**.

The solvent-accessible volume in **3** is increased up to ∼33.64% of the unit cell volume (Figure S15, Supporting Information), calculated from the crystal structure using the PLATON program.[48]

Strong $\pi-\pi$ interactions are present in hexagonal cavities of **4** and **5** along the *c* axis (Figure S16, Supporting Information). The metal to anion distance gets decreased in the case of **4**, and NO_3^- is placed between two binuclear clusters revealing strong hydrogen bonding with the hydrogens of imidazole moiety and central benzene ring of the ligand (Figure S17, Supporting Information). The metal to anion distance gets increased in **5** in comparison to **1** and anion is located in the center of the hexagonal cavity and the oxygen atom of acetone molecule is involved in hydrogen bonding interaction with the hydrogen of the central benzene ring as well as with the hydrogen of imidazole (Figure S18, Supporting Information).

The solvent accessible volume in **4** is increased to ∼34.3%, while in **5** it remains almost constant as in **1**.

Guest-exchange reactions were monitored by the powder X-ray diffraction technique. The similar PXRD patterns observed for the exchanged products are indicative of the fact that the entire framework is retained, throughout the SC−SC transformations mediated by solvent and anion-exchange processes (Figure 4, Scheme 2).

All the key parameters which have been altered during the guest exchange reactions have been summarized in the form of Tables S2 and S3 (Figure S19, Supporting Information).

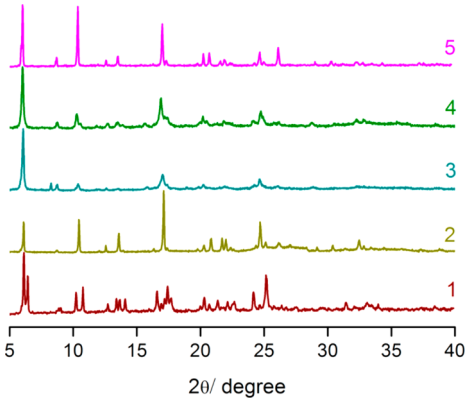

Figure 4. PXRD patterns for complexes **1**−**5**.

dx.doi.org/10.1021/cg500833s | *Cryst. Growth Des.* XXXX, XXX, XXX−XXX

Scheme 2. Schematic Representation of Guest Exchange within the Channels of 1

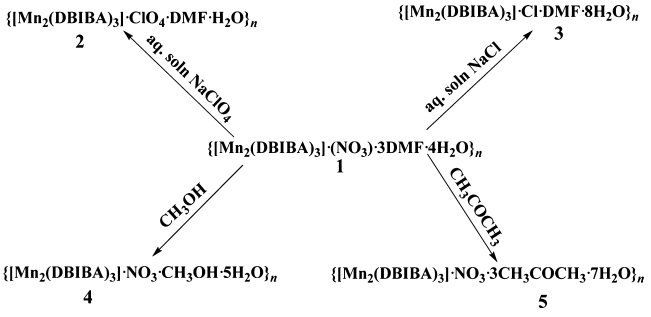

Thermogravimetric analysis of **1** shows a weight loss of ∼19% in the temperature range 35−290 °C, which corresponds to the loss of four water molecules and three DMF molecules (calcd 19.1%). After 370 °C, the complex starts decomposing (Figure S20). For compounds **2** and **3**, weight losses were found to be ∼11% and ∼13% respectively, which are equivalent to their lattice solvent molecules present in the framework. Decomposition takes place after 375 °C for complex **2** and after 400 °C for complex **3** (Figures S21−S22).

Gas Adsorption Studies. Gas adsorption measurements for N_2, H_2, and CO_2 gases were performed in a relative pressure range of 10^{-4} to 1 atm at 77 K (N_2 and H_2) and 195 K (CO_2) using activated compound prepared from **1**. Interestingly, the activated compound presented differential adsorption behavior toward CO_2 (195 K), as compared to those for N_2 (77 K) and H_2 (77 K). The CO_2 sorption profile was of a typical type-I nature with a significant uptake amount of 155 mL g^{-1} at 195 K, whereas both the N_2 and H_2-sorption plots refer to a typical type-III nature (with negligible gas-uptake excluding the high-pressure induced surface adsorption at $P/P_0 > 0.87$) (Figure 5a). Here, size selective uptake can certainly be ruled out because of the bigger pore size compared to the kinetic diameters of the probe-adsorptive gas species (CO_2 = 3.3 Å, N_2 = 3.64 Å, and H_2 = 2.8 Å).[50−52]

The type-III adsorption plots for N_2 and H_2 suggests a notably weak interaction between the sample surface of **1** and these adsorbate gas molecules possessing zero dipole moment. On the contrary CO_2, having a much larger quadruple moment (1.34×10^{-39} Cm^2), known to interact selectively with polar functionalities as compared to other gases registers a much higher adsorption-uptake with type-I profile, characteristic of strong interaction and also confirming the microporous nature of **1**. This striking low-temperature CO_2 selectivity further prompted investigation of the sorption performances for this material at room temperature (298 K), since the CO_2 adsorption amount at 273 K was experimentally found to be substantially high (73 mL g^{-1}) (Figure 5b). The uptake amounts for all the four gaseous probe species, namely, CO_2, N_2, H_2, and CH_4 could evidently present CO_2-selective adsorption phenomena even at room temperature, since the amounts adsorbed were 50 mL g^{-1} for CO_2, 14.6 mL g^{-1} for N_2, 23 mL g^{-1} for CH_4, and 3 mL g^{-1} for H_2 (Figure 6).

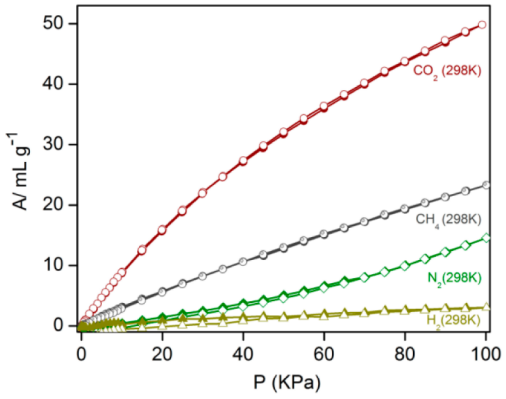

Figure 6. Adsorption isotherms of different gases (CO_2, CH_4, N_2, and H_2) at 298 K for **1** (filled shapes = adsorption, hollow shapes = desorption).

Since the adsorption amounts of other gases (H_2, N_2, and CH_4) are much smaller compared to CO_2, compound **1** can prove expedient for separation of CO_2 from a gas mixture at low to ambient temperature range. The Henry's law selectivities of CO_2/CH_4, CO_2/H_2, and CO_2/N_2 separation were calculated based on equation $S_{ij} = K_H(CO_2)/K_H(j)$.[53−56] (Table 2) The high CO_2/H_2 separation selectivity of ∼52.32 can be exploited in precombustion carbon capture and storage (CCS) technology, while CO_2/N_2 selectivity ∼66 makes it a prospective candidate for application in postcombustion CCS technology. The highly selective sorption of compound **1** solely

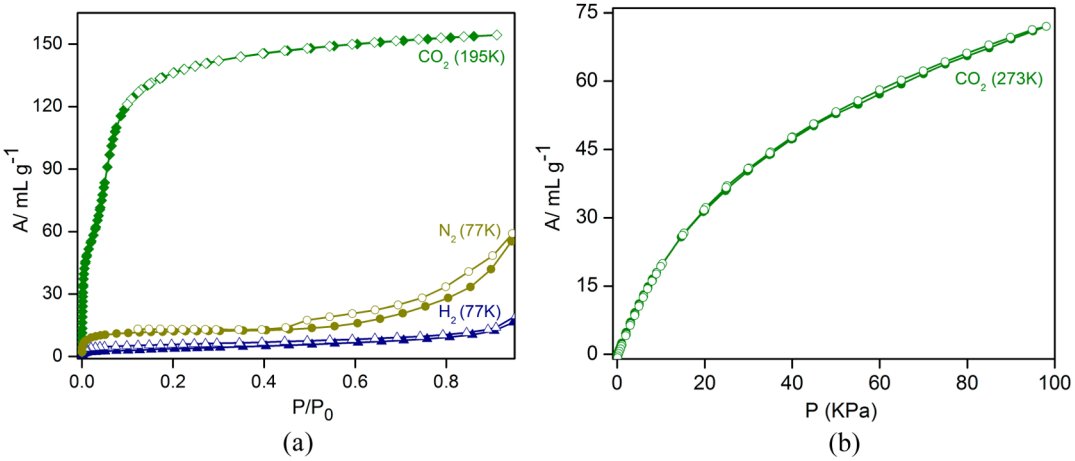

Figure 5. (a) Low temperature gas-adsorption profiles for **1**, amount adsorbed (in mL g^{-1}) plotted against P/P_0 and (b) CO_2 sorption isotherm at 273 K for complex **1** (filled shapes = adsorption, hollow shapes = desorption).

dx.doi.org/10.1021/cg500833s | Cryst. Growth Des. XXXX, XXX, XXX−XXX

Table 2. Virial Graph Analyses Data for Activated Compound 1 and Its CO_2/CH_4, CO_2/H_2, and CO_2/N_2 Separation Selectivities

temperature (K)	adsorbate	A_0 ln(mol g^{-1} Pa^{-1})	Henry's const K_H (mol g^{-1} Pa^{-1})	R^2	S_{ij}
298	CO_2	6.205×10^{-5}	6.205×10^{-5}	0.982	
298	CH_4	−11.321	1.211×10^{-5}	0.998	5.124
298	H_2	−13.645	1.186×10^{-6}	0.96	52.32
298	N_2	−13.878	9.393×10^{-7}	0.957	66.06

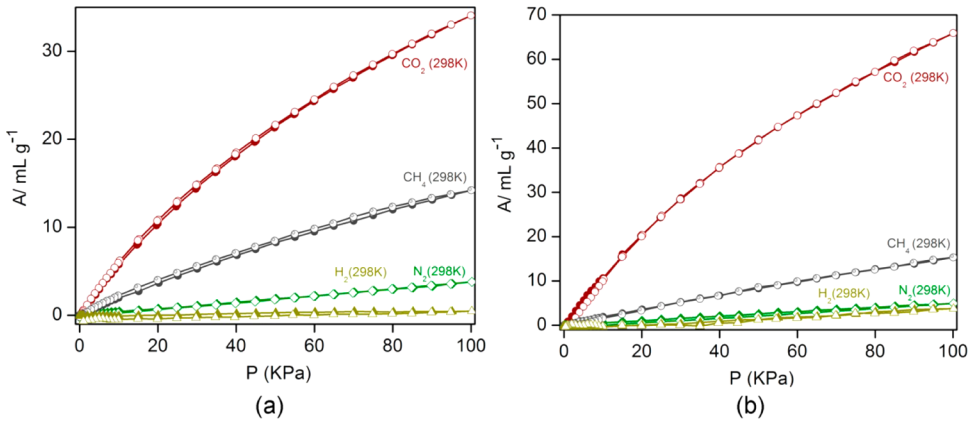

Figure 7. Adsorption isotherms of different gases (CO_2, CH_4, N_2, and H_2) at 298 K for (a) compound **2**, and (b) compound **3** (filled shapes = adsorption, hollow shapes = desorption).

to CO_2 at 298 K features the promise of this new microporous MOF for practical CO_2/H_2 and CO_2/N_2 separation in the near future. The isosteric heat of adsorption for CO_2 is found to be 27.4 kJ/mol for low loading (Figure S23, Supporting Information), as measured from CO_2-adsorption data plots at 273 and 298 K. BET surface area as calculated from CO_2 adsorption isotherm at 195 K was found to be 365.82 m^2 g^{-1}. The Haworth−Kawazoe (H−K) plot for CO_2 sorption at 195 K (Figure S24, Supporting Information) reveals an effective pore diameter of 8.4 Å, which is relatively larger than kinetic diameter for any of the probe gases. This further confirms the fact that size-selectivity between different probe gases is not the deciding factor; rather the selective uptake of CO_2 by **1** can be ascribed to the electrostatic interactions of CO_2 with nitrate anions and the carboxylate oxygens of the coordinated ligand. Phase purity of the sample was proven by PXRD measurements before and after activation (Figure S25, Supporting Information). After the activation process, framework is thereby confirmed to be devoid of any guest molecules.

In order to verify the role of anions inherently present in these newly reported MOFs **1**, **2**, and **3** on their gas adsorption properties and subsequently coming up with a comparative analysis, the sorption performances for both compounds **2** and **3** were also recorded at 298, 273, and 77 K, as measured for compound **1** (Figures S26−S29, Supporting Information). Since size of the concerned anions follow the trend: Cl^- < NO_3^- < ClO_4^-,[57,58] as anticipated, that desolvated compounds **1** (with NO_3^-), **2** (with ClO_4^-) and **3** (with Cl^-) exhibited the following CO_2-storage/uptake capacity at 298 K: compound **2** < **1** < **3**. Similar to compound **1**, both these anion-exchanged frameworks presented a significantly high CO_2 selectivity as compared to the other flue gases like N_2, H_2, and CH_4 (Figure 7).

The Henry's law selectivities of CO_2/CH_4, CO_2/H_2, and CO_2/N_2 separation were calculated for these two compounds also, following the same protocol as adopted for compound **1**, which presented substantially high separation selectivity values (S_{ij}) for CO_2 as compared to other gases (Tables S4 and S5), although the concerned values are lower as compared to compound **1**, making the pristine MOF **1** the best candidate to exhibit CO_2-selective separation at 298 K.

Magnetic Properties. Magnetic susceptibility data at an applied dc field of 0.3 T for **1** were collected in the 2−300 K temperature range. The plots of χT vs T and χ vs T are shown in Figure 8. The χT product has values of 9.16 cm^3 K mol^{-1} at

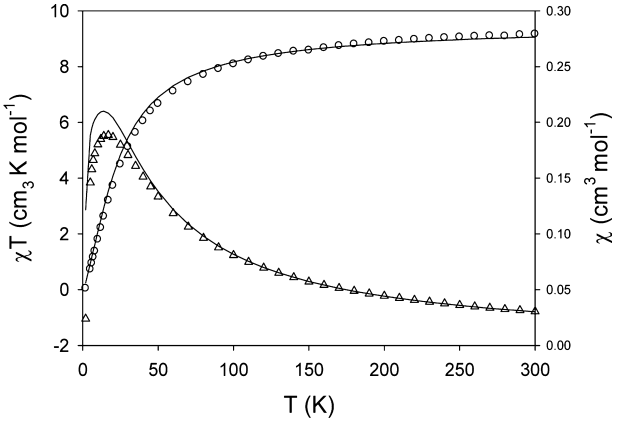

Figure 8. χT versus T (circles) and χ versus T (triangles, right axis) plots for **1** at an applied dc field of 0.3 T. The solid lines are the best fitting to a simplified model (see text for fitting parameters).

300 K. The observed value is slightly higher than that expected for two noninteracting Mn(II) ions with g = 2.0 and S = 5/2 of 4.375 × 2 = 8.75 cm^3 K mol^{-1}. As the temperature decreases, the χT product declines slightly, due to the Boltzmann depopulation of the excited states and simultaneous population of the antiferromagnetically coupled ground state. A maximum is observed in the χ versus T plot, indicating the population of

dx.doi.org/10.1021/cg500833s | Cryst. Growth Des. XXXX, XXX, XXX−XXX

(S = 0) spin ground state, antiferromagnetic order below the maximum T of 17 K. Since exchange constant is quite small between antiferromagnetically coupled Mn(II) dimers that is why antiferromagnetic order probably causes strong feature observed.

There are three well-defined structural motifs for **1**, which will have a great influence in the magnetic property. First, the binuclear Mn(II) unit is bridged by three *syn-syn* carboxylate groups with a distorted configuration (Figure 9), which are

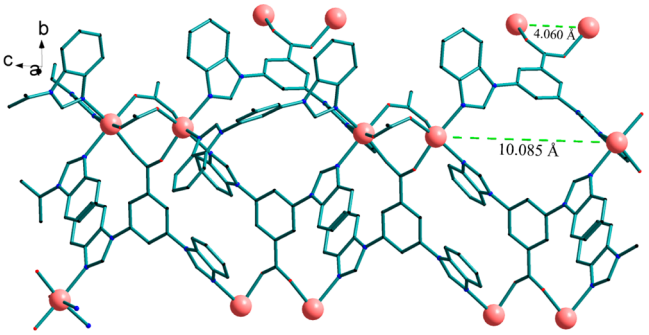

Figure 9. Simplified view along the *a* axis of the unit cell, showing the way Mn_2 units are linked by the ligand (the Mn−Mn distance within the binuclear unit is 4.0 Å, and between binuclear units 10.0 Å).

bent with torsion angles Mn−O−C−O′−Mn′ between 60° and 70°. The lack of planarity will affect the superexchange process through the delocalized π orbitals of carboxylate group, making it less effective and weaker. The second structural motif is the unique arrangement of chains assembled by *meta*-bis-imidazole phenyl groups, constituted from the linking of the binuclear units each one of these chains is a node in the basic hexagonal network (Figure 3a).

It is known that this type of *meta*-substituted phenyl rings can lead to weak ferromagnetic coupling, although this is unlikely with Mn(II).[59,60]

The susceptibility and magnetization data were fitted together using the software package PHI.[61] PHI is a computer package designed for the calculation and interpretation of the magnetic properties of paramagnetic compounds which uses a phenomenological Hamiltonian. This system is solved by evaluating the matrix elements of the Hamiltonian over the basis states and diagonalizing the Hamiltonian matrix. The model used to fit the magnetic data which considers that the magnetic binuclear Mn(II) units of **1** are isolated. This is based on the crystal structure of **1** which shows Mn−Mn intranuclear distance is 4.0 Å and distance between the binuclear clusters is 10.0 Å. Taking into account that Mn(II)−Mn(II) couplings are very weak, the best fits are shown as solid lines in Figures 8 and Figure S30. The best fitting parameters are g = 2.24 and J = −1.67 cm^{-1}. The deviation observed in the susceptibility plot at low temperatures can be attributed to the fact that interdimer interactions are not taken into account in the model, but these can be important at low temperature especially in a MOF where they propagate through the crystal.

CONCLUSION

In summary, a new 3D coordination polymer of Mn(II) (**1**) has been synthesized displaying anion/solvent exchange mediated development of four analogous isostructural coordination polymers (**2**−**5**) in a SC−SC fashion, with precise crystalline framework-retention during which supramolecular noncovalent interactions play an extremely crucial role. Guest-free activated phase of complexes **1**, **2**, and **3** exhibits the intriguing selective CO_2-sorption phenomena at low to ambient temperature and at low pressure regime. Magnetic measurements on **1** confirm a weak antiferromagnetic behavior below 17 K.

ASSOCIATED CONTENT

Supporting Information

X-ray crystallographic data in CIF format, table for selected bonds and distances for **1**−**5**, IR, TGA, and PXRD analysis. This material is available free of charge via the Internet at http://pubs.acs.org.

AUTHOR INFORMATION

Corresponding Author

*E-mail: pkb@iitk.ac.in.

Notes

The authors declare no competing financial interest.

ACKNOWLEDGMENTS

P.K.B. gratefully acknowledges the financial support received from the Department of Science and Technology, New Delhi, India. E.C.S. acknowledges the financial support from the Spanish Government (Grant CTQ2012-032247 and Ramón y Cajal contract). S.M. acknowledges IISER Pune for research facilities and funding.

REFERENCES

(1) Yaghi, O. M.; Li, H. *J. Am. Chem. Soc.* **1995**, *117*, 10401−10402.
(2) Kamiyama, A.; Noguchi, T.; Kajiwara, T.; Ito, T. *Angew. Chem., Int. Ed.* **2000**, *39*, 3130−3132.
(3) Uemura, K.; Kitagawa, S.; Kondo, M.; Fukui, K.; Kitaura, R.; Chang, H.-C.; Mizutani, T. *Chem.—Eur. J.* **2002**, *8*, 3587−3600.
(4) Mukherjee, S.; Joarder, B.; Manna, B.; Desai, A. V.; Chaudhari, A. K.; Ghosh, S. K. *Sci. Rep.* **2014**, *4*, No. 5761, DOI: 10.1038/srep05761.
(5) Rosi, N. L.; Eckert, J.; Eddaoudi, M.; Vodak, D. T.; Kim, J.; O'Keeffe, M.; Yaghi, O. M. *Science* **2003**, *300*, 1127−1129.
(6) Noro, S.; Kitagawa, S.; Kondo, M.; Seki, K. *Angew. Chem., Int. Ed.* **2000**, *39*, 2081−2084.
(7) Sahu, J.; Ahmad, M.; Bharadwaj, P. K. *Cryst. Growth Des.* **2013**, *13*, 2618−2627.
(8) Singh, R.; Ahmad, M.; Bharadwaj, P. K. *Cryst. Growth Des.* **2012**, *12*, 5025−5034.
(9) Halder, G. J.; Kepert, C. J.; Moubaraki, B.; Murray, K. S.; Cashion, J. D. *Science* **2002**, *298*, 1762−1765.
(10) Ahmad, M.; Sharma, M. K.; Das, R.; Poddar, P.; Bharadwaj, P. K. *Cryst. Growth Des.* **2012**, *12*, 1571−1578.
(11) Maspoch, D.; Ruiz-Molina, D.; Wurst, K.; Domingo, N.; Cavallini, M.; Biscarini, F.; Tejada, J.; Rovira, C.; Veciana, J. *Nat. Mater.* **2003**, *2*, 190−195.
(12) Gallo, M.; Glossnan-Mitnik, D. *J. Phys. Chem. C* **2009**, *113*, 6634−6642.
(13) Kitaura, R.; Seki, K.; Akiyama, G.; Kitagawa, S. *Angew. Chem., Int. Ed.* **2003**, *42*, 428−431.
(14) Chen, B.; Ma, S.; Zapata, F.; Fronczek, F. R.; Lobkovsky, E. B.; Zhou, H.-C. *Inorg. Chem.* **2007**, *46*, 1233−1236.
(15) Millward, A. R.; Yaghi, O. M. *J. Am. Chem. Soc.* **2005**, *127*, 17998−17999.
(16) Waldo, G. S.; Yu, S.; Penner-Hahn, J. E. *J. Am. Chem. Soc.* **1992**, *114*, 5869−5870.
(17) Tan, X. S.; Xiang, D. F.; Tang, W. X.; Sun, J. *Polyhedron* **1997**, *16*, 689−694.
(18) Policar, C.; Lambert, F.; Cesario, M.; Morgenstern-Badarau, I. *Eur. J. Inorg. Chem.* **1999**, 2201−2207.
(19) Delgado, F. S.; Kerbellec, N.; Ruiz-Perez, C.; Cano, J.; Lloret, F.; Julve, M. *Inorg. Chem.* **2006**, *45*, 1012−1020.

(20) Meng, M.; Zhong, D.-C.; Lu, T. B. *CrystEngComm* **2011**, *13*, 6794−6800.
(21) Lampropoulos, C.; Redler, G.; Data, S.; Abboud, K. A.; Hill, S.; Christou, G. *Inorg. Chem.* **2010**, *49*, 1325−1336.
(22) Berggren, G.; Huang, P.; Eriksson, L.; Styring, S.; Anderlund, M. F.; Thapper, A. *Dalton Trans.* **2010**, *39*, 11035−11044.
(23) Li, Y.; Zou, W. Q.; Wu, M. F.; Lin, J. D.; Zheng, F. K.; Liu, Z. F.; Wang, S. H.; Guo, G. C.; Huang, J. S. *CrystEngComm* **2011**, *13*, 3868−3877.
(24) Wang, Y. Q.; Sun, Q.; Yue, Q.; Cheng, A. L.; Song, Y.; Gao, E. Q. *Dalton Trans.* **2011**, *40*, 10966−10974.
(25) Wang, X. F.; Zhang, Y. B.; Zhang, W. X.; Xue, W.; Zhou, H. L.; Chen, X. M. *CrystEngComm* **2011**, *13*, 4196−4201.
(26) Ma, C. B.; Hu, M. Q.; Chen, H.; Wang, M.; Zhang, C. X.; Chen, C. N.; Liu, Q. T. *CrystEngComm* **2010**, *12*, 1467−1473.
(27) Chen, W. X.; Zhuang, G. L.; Zhao, H. X.; Long, L. S.; Huang, R. B.; Zheng, L. S. *Dalton Trans.* **2011**, *40*, 10237−10241.
(28) Janiak, C. *Dalton Trans.* **2003**, 2781−2804.
(29) Coronado, E.; Palacio, F.; Veciana, J. *Angew. Chem.* **2003**, *115*, 2674−2676; *Angew. Chem., Int. Ed.* **2003**, *42*, 2570−2572.
(30) Kahn, O. *Molecular Magnetism*; VCH: New York, 1993.
(31) Zhou, X. P.; Zhang, X. J.; Lin, S. H.; Li, D. *Cryst. Growth Des.* **2007**, *7*, 485−487.
(32) Jung, O. S.; Park, S. H.; Kim, K. M.; Jang, H. G. *Inorg. Chem.* **1998**, *37*, 5781−5785.
(33) Withersby, M. A.; Blake, A. J.; Champness, N. R.; Cooke, P. A.; Hubberstey, P.; Li, W. S.; Schröder, M. *Inorg. Chem.* **1999**, *38*, 2259−2266.
(34) Chen, H. B.; Zhang, H.; Yang, J. M.; Zhou, Z. H. *Polyhedron* **2004**, *23*, 987−991.
(35) Sun, W. Y.; Fan, J.; Okamura, T. A.; Xie, J.; Yu, K. B.; Ueyam, N. *Chem.—Eur. J.* **2001**, *7*, 2557−2562.
(36) Fan, J.; Gan, L.; Kawaguchi, H.; Sun, W. Y.; Yu, K. B.; Tang, W. X. *Chem.— Eur. J.* **2003**, *9*, 3965−3973.
(37) Liu, H. K.; Huang, X. H.; Lu, T. H.; Wang, X. J.; Sun, W. Y.; Kang, B. S. *Dalton Trans.* **2008**, 3178−3188.
(38) Reger, D. L.; Semeniuc, R. F.; Rassolov, V.; Smith, M. D. *Inorg. Chem.* **2004**, *43*, 537−554.
(39) Sarkar, M.; Biradha, K. *Cryst. Growth Des.* **2006**, *6*, 1742−1745.
(40) Dalrymple, S. A.; Shimizu, G. K. H. *Chem.—Eur. J.* **2002**, *8*, 3010−3015.
(41) Qiu, Y. C.; Liu, Z. H.; Li, Y. H.; Deng, H.; Zeng, R. H.; Zeller, M. *Inorg. Chem.* **2008**, *47*, 5122−5128.
(42) Wang, Y.; Cheng, P.; Song, Y.; Liao, D. Z.; Yan, S. P. *Chem.—Eur. J.* **2007**, *13*, 8131−8138.
(43) Kitagawa, S.; Matsuda, R. *Coord. Chem. Rev.* **2007**, *251*, 2490−2509.
(44) Nouar, F. N.; Eubank, J. F.; Bousquet, T.; Wojtas, L.; Zaworotko, M. J.; Eddaoudi, M. *J. Am. Chem. Soc.* **2008**, *130*, 1833−1835.
(45) Zhai, Q. G.; Wu, X. Y.; Chen, S. M.; Zhao, Z. G.; Lu, C. Z. *Inorg. Chem.* **2007**, *46*, 5046−5058.
(46) König, E. *Magnetic Properties of Coordination and Organometallic Transition Metal Compounds*; Springer: Berlin, 1966.
(47) Agarwal, R. A.; Aijaz, A.; Ahmad, M.; Sañudo, E. C.; Xu, Q.; Bharadwaj, P. K. *Cryst. Growth Des.* **2012**, *12*, 2999−3005.
(48) Spek, A. L. *PLATON*; The University of Utrecht: Utrecht, The Netherlands, 1999.
(49) Agarwal, R. A.; Aijaz, A.; Sañudo, E. C.; Xu, Q.; Bharadwaj, P. K. *Cryst. Growth Des.* **2013**, *13*, 1238−1245.
(50) Férey, G.; Serre, C.; Devic, T.; Maurin, G.; Jobic, H.; Llewellyn, P. L.; Weireld, G. D.; Vimont, A.; Daturi, M.; Chang, J.-S. *Chem. Soc. Rev.* **2011**, *40*, 550−562.
(51) Nagarkar, S. S.; Chaudhari, A. K.; Ghosh, S. K. *Inorg. Chem.* **2012**, *51*, 572−576.
(52) Chaudhari, A. K.; Mukherjee, S.; Nagarkar, S. S.; Joarder, B.; Ghosh, S. K. *CrystEngComm* **2013**, *15*, 9465−9471.
(53) Keskin, S.; Heest, T. M. V.; Sholl, D. S. *ChemSusChem.* **2010**, *3*, 879−891.
(54) Chen, Z.; Xiang, S.; Arman, H. D.; Mondal, J. U.; Li, P.; Zhao, D.; Chen, B. *Inorg. Chem.* **2011**, *50*, 3442−3446.
(55) Roswell, J.; Yaghi, O. M. *J. Am. Chem. Soc.* **2006**, *128*, 1304−1315.
(56) Xiang, S. C.; Zhou, W.; Gallegos, J. M.; Liu, Y.; Chen, B. *J. Am. Chem. Soc.* **2009**, *131*, 12415−12419.
(57) Santucci, R.; Bongiovanni, C.; Mei, G.; Ferri, T.; Polizio, F.; Desideri, A. *Biochemistry* **2000**, *39*, 12632−12638.
(58) Richards, L. A.; Schaefer, A.; Richards, B. S.; Corry, B. *Small.* **2012**, *8*, 1701−1709.
(59) Laye, R. H.; Sañudo, E. C. *Inorg. Chim. Acta* **2009**, *362*, 2205−2212.
(60) Paital, A. R.; Mitra, T.; Ray, D.; Wong, W. T.; Ribas-Ariño, J.; Novoa, J. J.; Ribasa, J.; Aromı, G. *Chem. Commun.* **2005**, 5172−5174.
(61) Chilton, N. F.; Anderson, R. P.; Turner, L. D.; Soncini, A.; Murray, K. S. *J. Comput. Chem.* **2013**, *34*, 1164−1175.